

## **APPLICATION OF ELECTRONIC SPECKLE PATTERN INTERFEROMETRY (ESPI) TO OBSERVE THE FRACTURE PROCESS ZONE**

E. Hack,  
Swiss Federal Laboratories for Materials Testing and Research,  
Dubendorf, Switzerland  
T. Steiger, and H. Sadouki,  
Laboratory for Building Materials, Swiss Federal Institute of Technology,  
Zurich, Switzerland

### **Abstract**

3D-ESPI was used to monitor in real-time the crack growth and fracture process zone of polymer concrete and polymer mortar wedge splitting test specimens. The characteristics of the visualized deformation field provide the possibility to determine real and fictitious crack length, crack growth and crack opening under increasing displacement. Parameters of non-linear fracture mechanics which were deduced from experimental load-displacement curves were used in the fictitious crack model to numerically simulate the crack propagation. It is shown that within different load increments the applied crack model provides real and fictitious crack lengths close to the values determined experimentally by the 3D-ESPI analysis. Therefore, by means of the ESPI method the applicability of the fictitious crack model can be justified.

### **1 Introduction**

The accurate description of cracking in heterogeneous materials such as polymer concrete requires the use of non-linear fracture mechanics models which take into account the existence of a fracture process zone

(FPZ) in front of the crack tip. The determination of the extension of FPZ in composite materials is a considerably difficult experimental problem. Non-contacting and imaging techniques based on laser interference are often applied (Jacquot (1984)), e.g. ESPI (Rostasy and Laube (1990), Jia and Shah (1994)), holographic moiré (Rastogi and Denarié (1994)), speckle pattern photography (Horii and Ichinomiya (1991)). The visualized deformation fields provide the possibility to determine real and fictitious crack length, crack growth and crack opening under increasing load. The 3D-ESPI-technique used in this work offers the possibility to measure in- and out-of-plane displacement fields of the material surface. The observation of correlation fringes in real-time on a TV-monitor allows a qualitative survey of the crack growth, while phase shift techniques and image processing are used for quantitative analysis. The aim of this contribution is to validate a fracture mechanics model for polymer composites by means of the ESPI-method.

## 2 Fracture mechanics model and FE-analysis

Polymer concrete is composed of aggregates following a given size distribution dispersed in a polymer binding matrix. Intensive experimental investigations were performed on polymer concrete specimens to study the fracture process. The analysis of the results showed that the fracture behaviour of polymer concrete is very similar to those of cement composite materials. The total load-displacement responses (pre- and post-peak) obtained are comparable to the responses relative to normal concrete. Optical techniques such as ESPI used to investigate crack formation and crack propagation revealed that a small damaged zone is formed at the real crack tip before further propagation of the real crack occurs. Owing to these observations, it can be deduced that polymer concrete can not be considered as a brittle material but rather as a strain-softening material. Cohesive-crack based models are most suitable to describe the fracture process in these composite materials. In this work the fictitious crack model (FCM) developed by Hillerborg (Hillerborg et al. (1976)) to describe the failure process in cementitious composites was adopted as a first approach. The damaged zone or FPZ is characterized by its tensile stress transfer capability which decreases gradually as the FPZ develops under increasing load. At a given critical widening of the FPZ, the stress transfer falls to zero, and a real crack occurs. The mechanical properties of the FPZ are described by the so-called strain softening curve (Fig.1).

Two principal strategies can be followed to perform a numerical simulation of the fracture process based on the FCM concept: discrete crack and smeared crack approaches. In the following, discrete crack technique combined with FEM is used (FRACT1). For the sake of simplicity the

Table 1. Strain-softening parameters

E	G <sub>f</sub>	f <sub>t</sub>	σ <sub>1</sub>	w <sub>1</sub>	w <sub>2</sub>
N/mm <sup>2</sup>	N/m	MPa	MPa	mm	mm
39000	240	12.4	2.73	0.03	0.04

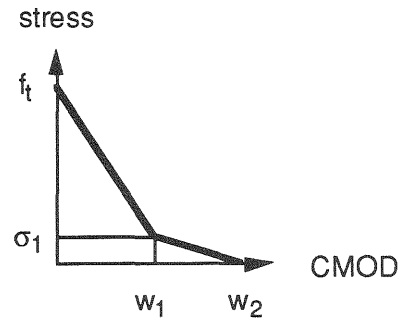


Fig. 1. Strain-softening diagram

strain-softening diagram as shown in Fig.1 is modelled by a bilinear curve defined by four material parameters ( $f_t$ ,  $\sigma_1$ ,  $w_1$  and  $w_2$ ). Table 1 gives the relevant mechanical parameters obtained for polymer concrete. The area under the curve is the specific fracture energy ( $G_f$ ) given by the following relationship:

$$G_f = 0.5 \cdot (f_t \cdot w_1 + \sigma_1 \cdot w_2) \quad (1)$$

In principle the strain softening diagram can be directly obtained by uniaxial tension tests, but unfortunately these tests are often difficult to perform. For that reason, the strain-softening diagram is derived by using load-displacement response obtained on WST-specimens combined with an adequate inverse analysis (Roelfstra and Wittmann (1986)).

### 3 ESPI measurement technique

ESPI (Electronic Speckle Pattern Interferometry) is an interferometric technique to measure deformation vector fields of diffusely scattering objects (Jones and Wykes (1989)). The reflected laser light shows a stochastic, granular intensity pattern which is determined by the microstructure of the object surface. In an ESPI-interferometer the reflected light is superposed to a reference beam. The resulting interference pattern measures the light path difference between the two beams in multiples of the laser wavelength  $\lambda$ . Comparing the interference patterns recorded by a CCD-camera before and after an object displacement allows to measure the deformation. By illuminating the object from different directions all three components of the displacement vector ( $u, v, w$ ) between two load states can be obtained and displayed as lines of equal displacement as illustrated by Fig.2. Rigid body movements (rotations and translations) can be corrected for by adding synthetic fringe patterns to the phase maps. For the determination of strain increments the in-plane results are used.

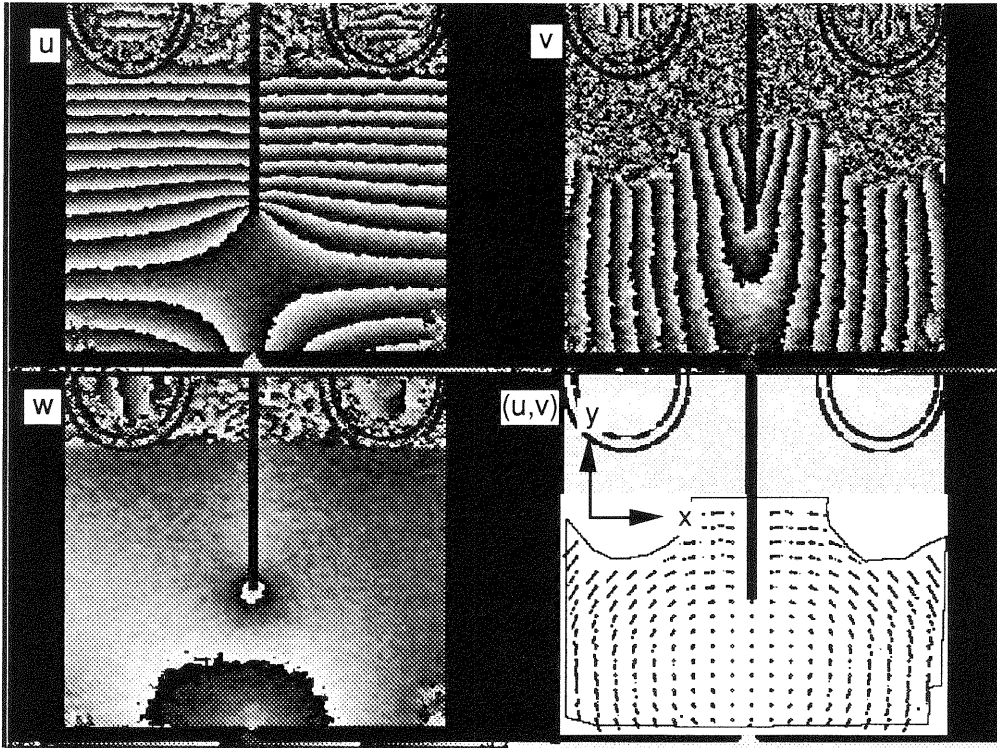


Fig. 2. 3D-ESPI analysis. Phase maps representing lines of equal x-, y-, and z-displacements, respectively, and the vector diagram for the in-plane (x,y)-displacement .

The out-of-plane measurement can give clues to e.g. bending of test specimen and transverse contraction.

## 4 Experiments

### 4.1 Tests on polymer concrete specimens

The required fracture mechanics properties of polymer concrete were determined from wedge splitting tests (Fig.3). Wedge splitting was used in order to obtain stable crack growth during the fracture process. A specimen of size  $300 \times 300 \times 80 \text{ mm}^3$  with a ligament of  $h_0 = 104 \text{ mm}$  was prepared and tested on a Zwick loading machine. The material is composed of 15 vol% of an epoxy resin hardener system and 85 vol% of crushed aggregates with sizes following a Fuller distribution. The applied load and the crack mouth opening displacement (CMOD) were recorded. The velocity was held constant at  $12 \text{ } \mu\text{m/s}$ . The resulting load-displacement curve was analysed numerically to find the relevant parameters (see Table 1).

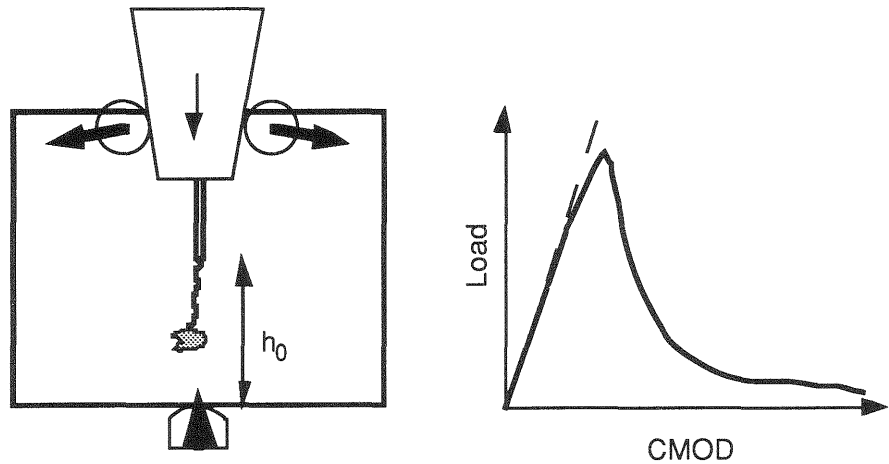


Fig. 3. Wedge splitting test specimen (schematic), and typical load-displacement curve.

A 3D-ESPI interferometer was mounted to the Zwick testing machine. The specimen was illuminated sequentially from three directions (Fig.4) by an argon ion laser run on a water-air heat exchanger. Frame grab was performed without stopping the machine in regular intervals. The measurements of the incremental displacement vector were performed on an area of  $190 \times 140 \text{ mm}^2$  using a phase shift technique. The resulting phase maps have sensitivities of  $0.52 \text{ } \mu\text{m}$  per fringe in-plane ( $x, y$ ) and  $0.44 \text{ } \mu\text{m}$  per fringe out-of-plane ( $z$ ) given by the illumination angle  $\theta$ .

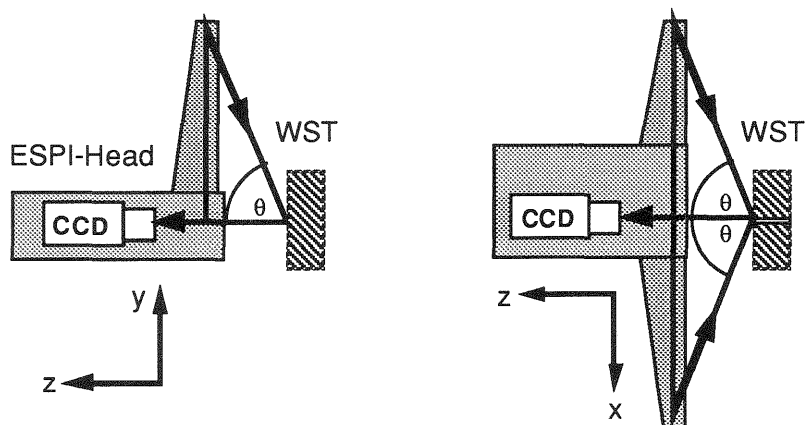


Fig. 4. Illumination (schematic) of the wedge splitting test specimen (WST), and definition of axes.

## 4.2 Tests on polymer mortar specimens

To complement the measurements on the Zwick machine experiments on polymer mortar specimens of size  $30 \times 30 \times 5 \text{ mm}^3$  (35 vol% fine aggregates with  $d_{\max} \leq 0.2 \text{ mm}$  and 65 vol% epoxy resin hardener system) were performed in the laboratory on a vibration isolated optical table. The tests were performed on a modified tensile stage normally used for in-situ experiments in an environmental scanning electron microscope (Steiger et al. (1995)).

## 5 Comparison of numerical and experimental results

### 5.1 Identification of parameters from ESPI fringe patterns

The real crack is characterized by sharply broken fringes. The *crack tip*, therefore, can be localized at the end of this region. Broken fringes correspond to discontinuities in the displacement field and are visible, in general, within any component of the displacement vector.

The FPZ is characterized by the appearance of microcracks on the surface which can also be observed as broken fringes on a microscopic scale. Fig.5 illustrates such a determination of FPZ on a polymer mortar

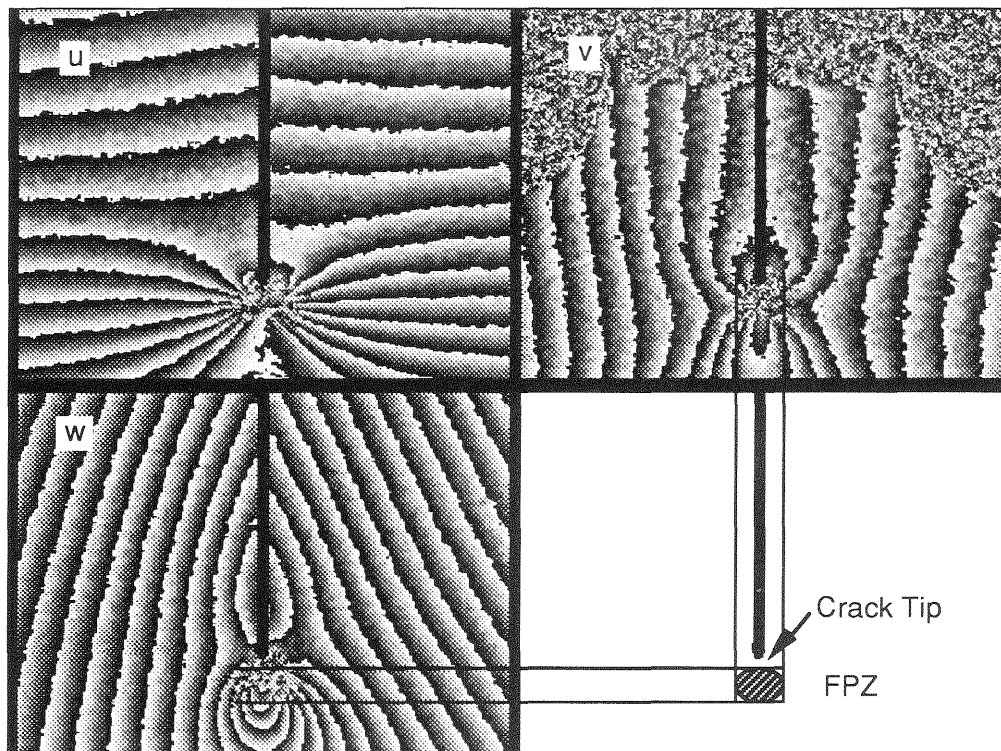


Fig. 5 Determination of FPZ at the beginning of cracking in polymer mortar. The field of view is  $18 \times 14 \text{ mm}^2$ .

specimen. However, many microcracks cannot be identified owing to the speckle effect and the limited lateral resolution of the CCD-camera.

To obtain a more reliable criterion for the identification of the FPZ we consider *neutral lines* defined as lines of  $\sigma=0$  in case of linear elasticity and small strains. For an ideal horizontal bending beam this corresponds to  $\Delta u=0$ , and, consequently,  $\Delta \epsilon=0$  under increasing load. Computational shearing of the image of  $\Delta u$  in x-direction results in an image representing the strain increment since  $\partial \Delta u / \partial x = \Delta(\partial u / \partial x) = \Delta \epsilon$ . Lines of  $\Delta \epsilon=0$  in the computer sheared image separate regions of increasing strain from regions of gradual unloading and compression (Fig.6.). These lines are sharply defined. The advantage of the determination of crack propagation from neutral lines is that they do not depend on surface microcracks, but on bulk behaviour. Fig.7 gives the relation to the FPZ.

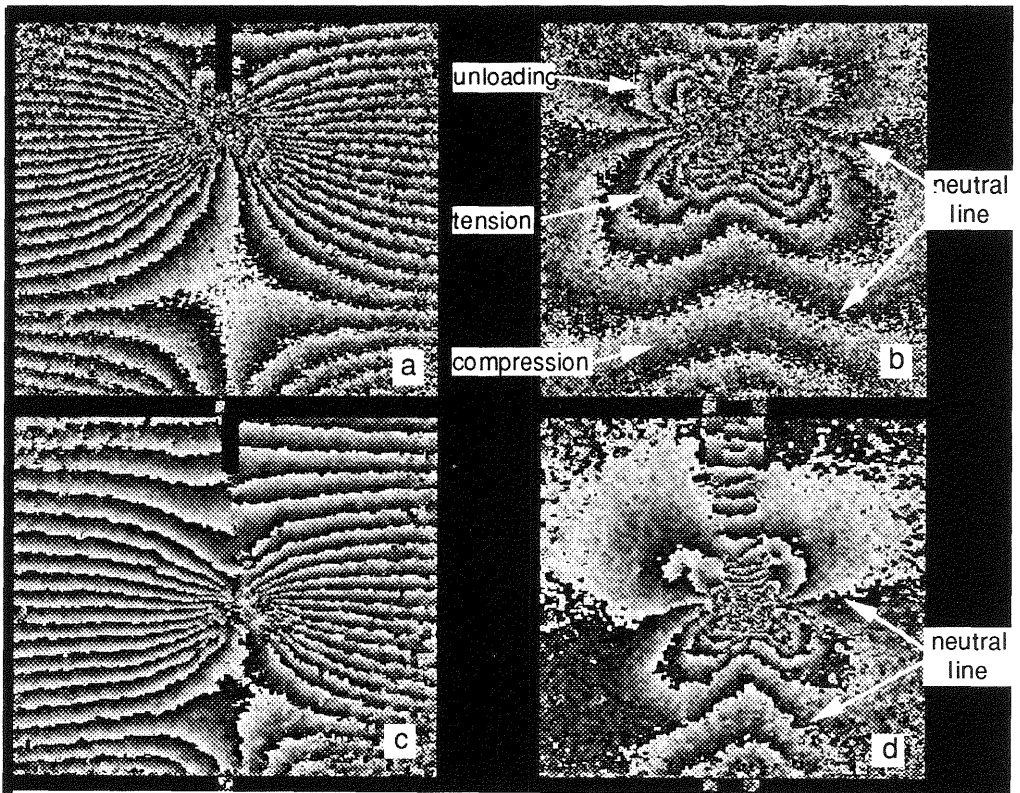


Fig. 6. Displacement component  $\Delta u$  at peak load of 6.8 kN (a) and at post-peak load of 3.9 kN (c) with the computer sheared images (b) and (d), respectively.

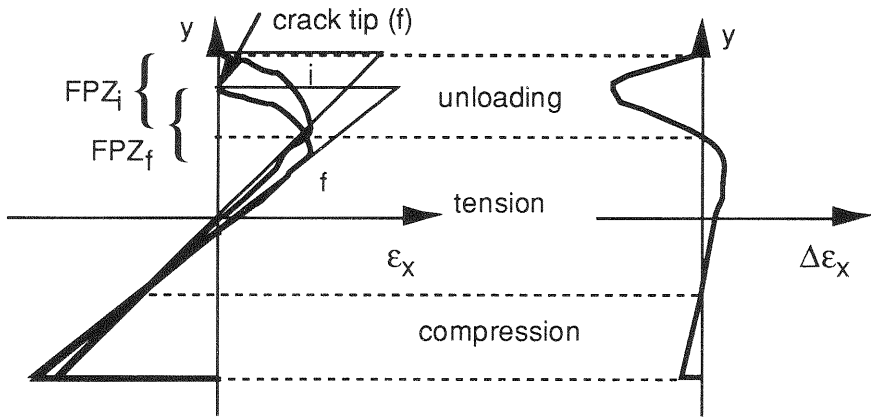


Fig. 7. Evolution of the strain profile between initial (i) and final (f) state under increasing load and in presence of a real crack.

## 5.2 Comparison of numerical and experimental results

The length of the real crack, the total crack and the position of the neutral line are depicted in fig.8. The length of the real crack and the FPZ have

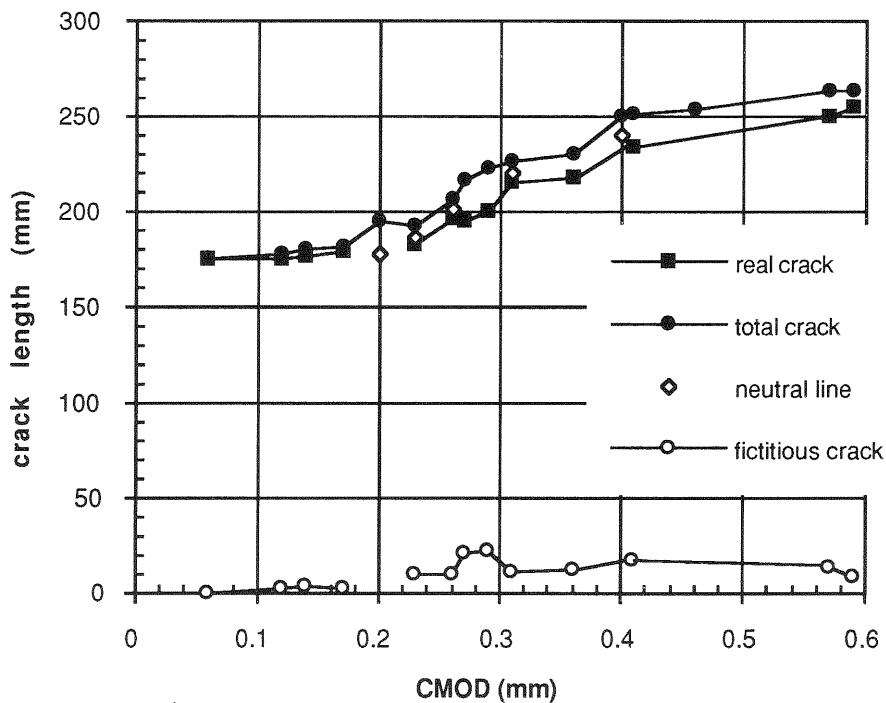


Fig. 8. Crack growth parameters determined from ESPI-measurements.

been evaluated from the fringe patterns of one illuminating direction, while the position of the neutral line was determined from the computer-sheared image of x-displacement phase maps (shear-width of 50 pixels). In Fig. 9 the experimental load–displacement curve and the calculated crack lengths are shown. The displacement increment highlighted by the two vertical lines results in the ESPI fringe pattern depicted in fig. 6c.

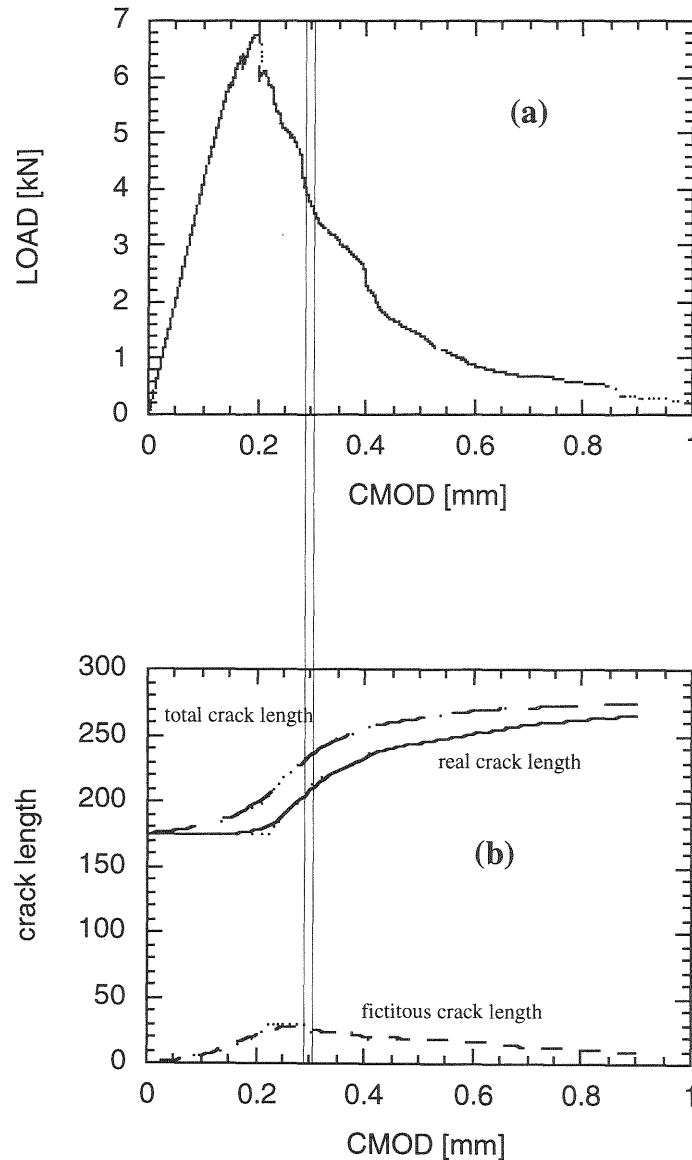


Fig. 9. Measured load-displacement curve (a) and the calculated crack lengths (b) for the polymer concrete specimen.

## 6 Conclusions

It could be shown that within different load increments the applied crack model provides nearly the same real and fictitious crack lengths as determined experimentally by a 3D-ESPI analysis. On the other hand one can state that by means of the ESPI method the fictitious crack model can be justified.

## References

- Hillerborg, A., Mod er, M., and Petersson, P.E. (1976) Analysis of crack formation and crack growth in concrete by means of fracture mechanics and finite elements, **Cement and Concrete Res.** 6, 773–782.
- Horii, H., and Ichinomiya, T. (1991) Observation of fracture process zone by laser speckle technique and governing mechanism in fracture of concrete, **Int. J. of Fracture** 51, 19–29.
- Jacquot, P. (1984) Interferometry in scattered coherent light applied to the analysis of cracking in concrete, in **Fracture mechanics of concrete: Material characterization and testing** (eds A.Carpinteri and A.R. Ingrassia), Martinus Nijhoff, Den Haag, 161–194.
- Jia, Z., and Shah, S.P. (1994) Two-dimensional Electronic-speckle-pattern Interferometry and Concrete-fracture Processes, **Exp. Mech.** 34, 262–270.
- Jones, R., and Wykes, C. (1989) **Holographic and Speckle Interferometry**, 2nd ed., Cambridge University Press, Cambridge.
- Rastogi, P.K., and Denari , E. (1994) Measurement of the length of fracture process zone in fiber-reinforced concrete using holographic moir , **Exp. Techn.** 18, 4, 11–17.
- Roelfstra, P.E., and Wittmann, F.H. (1986) Numerical method to link strain softening with failure of concrete, in: **Fracture toughness and fracture energy of concrete** (ed F.H. Wittmann), Elsevier, Amsterdam, 163–175.
- Rostasy, F.S., and Laube, M. (1990) Zur laserinterferometrischen Vermessung der Rissprozesszone des Betonzugbruches, Festschrift zum 60. Geb. R. Springenschmid,  berreicht durch Newport Instruments
- Steiger, T., Sadouki, H., and Wittmann, F.H. (1995) Simulation and observation of the fracture process zone, in: **FRAMCOS-2**, same volume